Multiscale modeling of two-dimensional contacts

B. Q. Luan,[1] S. Hyun,[2] J. F. Molinari,[3] N. Bernstein,[4] and Mark O. Robbins[1,3]
[1]*Department of Physics and Astronomy, The Johns Hopkins University, 3400 N. Charles Street, Baltimore, Maryland 21218, USA*
[2]*School of Mechanical Engineering, Kyungpook National University, Daegu, 702-701, Korea*
[3]*Department of Mechanical Engineering, The Johns Hopkins University, 3400 N. Charles Street, Baltimore, Maryland 21218, USA*
[4]*Center for Computational Materials Science, Naval Research Laboratory, Washington, DC 20375, USA*
(Received 10 March 2006; published 30 October 2006)

A hybrid simulation method is introduced and used to study two-dimensional single-asperity and multiasperity contacts both quasistatically and dynamically. The method combines an atomistic treatment of the interfacial region with a finite-element method description of subsurface deformations. The dynamics in the two regions are coupled through displacement boundary conditions applied at the outer edges of an overlap region. The two solutions are followed concurrently but with different time resolution. The method is benchmarked against full atomistic simulations. Accurate results are obtained for contact areas, pressures, and static and dynamic friction forces. The time saving depends on the fraction of the system treated atomistically and is already more than a factor of 20 for the relatively small systems considered here.

DOI: 10.1103/PhysRevE.74.046710 PACS number(s): 02.70.−c, 45.10.−b, 46.55.+d

I. INTRODUCTION

Continuum theories [1] are widely used to analyze mechanical contact between surfaces. However, the assumptions of continuum theory lead to unphysical results, such as stress singularities at the edge of contacts. It is also troubling that recent continuum studies of rough surfaces [2,3] find that the contacts are always dominated by the smallest length scales that are included in the calculation. Recent atomistic studies of contact [4–6] reveal that atomic-scale roughness can lead to substantial deviations from continuum theory at nanometer scales.

Molecular dynamics (MD) simulations are capable of modeling the detailed atomic structure at contacting interfaces. However, the size of the systems that can be treated is limited. Recent studies of single-asperity contacts [5,6] approach the limits of system sizes that can be treated on dedicated parallel compute clusters. Treating a statistical distribution of asperities on rough surfaces requires new approaches. One possibility is to recognize that atomistic detail is only required in interfacial regions. Away from the interface, strains are small and change continuously. A continuum description, such as the finite-element method (FEM), can be applied there. The challenge is to develop algorithms that couple atomistic and continuum descriptions in different regions. For studies of contact and friction, these algorithms should be able to simultaneously treat finite temperature, dynamic systems, complex geometries, and nonlinear constitutive laws in the continuum.

A variety of approaches for concurrently coupling multiple computational methods have been developed in the last decade [7–25]. One class of methods constructs an approximate energy from a combination of atomistic and continuum terms [14]. One of the most powerful is the quasicontinuum method (QCM) [7,8]. In regions of small strain gradients, only a few atoms are followed, and the energy associated with the remaining atoms is obtained by assuming an affine displacement field. In regions where the strain gradients are large, the mesh is refined until each node corresponds to one atom and the QCM reduces to MD. The coupling formulation is based on nodal forces obtained as the derivatives of the potential energy functional, and the interface between the two types of regions has proven challenging to treat consistently. The original versions of this method are restricted to zero temperature and quasistatic processes, which limits their applicability to friction. Recently, progress has been made towards including finite temperatures [9]. In the coupling of length scales (CLS) method [12] there is a single layer of boundary atoms and nodes and a single total energy is defined for the whole system. One important limitation is that defining this energy for general geometries and interatomic potentials is not straightforward.

Another class of approaches integrates out fine-scale degrees of freedom approximately before the simulation begins. Finite temperature and dynamics have been implemented in coarse-graining methods by including an approximation to the energy and entropy of eliminated atoms [11] or by defining effective Hamiltonians in analogy to two-dimensional real-space renormalization group methods [10]. However, these approaches are difficult to extend to arbitrary interactions and/or higher dimensions. The bridging-scale method [13] uses a finite-element treatment in coarse-grained regions and treats the effect of eliminated atoms at linear order, leading to a memory kernel coupling all atoms that interact with eliminated atoms. Cai *et al.* [24] present a numerical method for obtaining a similar kernel that represents the effect of the entire outer region, assuming linear response. The computational overhead associated with calculating and using these memory kernels can be substantial. E and Huang have proposed a method for obtaining approximate local kernels for linear systems at zero temperature [25], which has been used to treat fracture and friction [26,27].

A third class of approaches couples atomistic and continuum regions through constraints on displacements, rather than constructing an approximate Hamiltonian. The finite-element and atomistic (FEAt) method [15] and coupled atomistics and discrete dislocation (CADD) method [28] refine the continuum mesh to atomic scales. The outer atoms feel

forces from "pad atoms" that follow the finite-element nodes and constrain the displacements of the outer nodes. The FEAt algorithm uses a nonlocal continuum formulation to include corrections from long-range interactions and a nonlinear treatment of the constitutive law. CADD simplifies these aspects of the model but includes the motion of dislocations through the atomistic-continuum boundary and has recently been extended to dynamic, finite-temperature simulations [29].

Our approach is closely related to this last class of methods and to recent work on coupling atomistic and continuum treatments of fluids [16–19]. Interfacial regions are described atomistically and bulk regions with the FEM. The dynamics in the two regions evolve concurrently, but with different time steps. The smallest mesh size is larger than the interaction range to minimize the need for a nonlocal treatment of the continuum and simplify the treatment of finite temperatures. In contrast to FEAt and CADD, the displacement boundary conditions are applied at separated interfaces and the MD and FEM descriptions overlap and evolve independently between these interfaces. At the outer edge of the MD region, atomic displacements are determined by interpolating strain fields from the FEM. A spatial and temporal average of atomic displacements provides nodal displacements at the boundary of the FEM region. The method can be applied to dynamic problems at finite temperature with any constitutive law and there is no constraint on the relative positions of nodes and atoms.

In Sec. II, we describe the atomistic and continuum methods used as well as the mechanism for coupling them together. Section III A describes tests of the hybrid method in quasistatic contact between single asperities and self-affine surfaces. Dynamic simulations of pulse propagation and sliding friction are described in Sec. III B. Section IV presents a summary and conclusions.

II. HYBRID METHOD

To illustrate the method we study single-asperity and multi-asperity contact in two dimensions. In each case the top solid is rigid and the bottom solid is deformable. In continuum mechanics, this situation can be mapped to contact between two elastic solids [1]. Periodic boundary conditions are applied along the interface of length L, and the bottom of the substrate is held fixed at depth D.

For each geometry, results from the hybrid method are compared to fully atomistic simulations. The next subsection provides details of the methods used in the atomistic simulations and the atomistic portion of the hybrid method. Then the continuum portion of the hybrid method is described, and the final subsection explains how the two descriptions are coupled. For the system sizes studied in this paper, the hybrid method is more than 20 times faster than the pure MD simulations used to validate it. The performance enhancement increases with system size, which has recently allowed us to treat much larger systems than would be feasible with purely atomistic simulations [4].

A. Atomistic simulations

The interactions between atoms within the deformable substrate are described by a truncated and shifted Lennard-Jones (LJ) potential V^{LJ}:

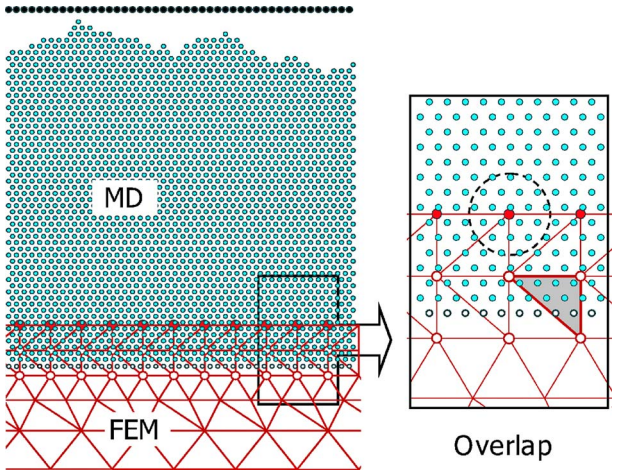

FIG. 1. (Color online) Hybrid model for contact between a rigid flat solid (black circles) and a rough elastic substrate (light blue circles). In the overlap region (magnified), outer nodes (large solid circles) deform according to the displacements of MD atoms within a radius r_{av} (dotted circle) and displacements of inner nodes (large open circles) control the motion of MD boundary atoms (small open circles) that lie within their element (shaded triangle). The FEM mesh size is about 4σ in the overlap and coarsens below.

$$V^{LJ}(r) = 4\epsilon\left[\left(\frac{\sigma}{r}\right)^{12} - \left(\frac{\sigma}{r}\right)^{6} - \left(\frac{\sigma}{r_c}\right)^{12} + \left(\frac{\sigma}{r_c}\right)^{6}\right] \quad (r < r_c), \tag{1}$$

where ϵ and σ are characteristic energy and length scales, respectively. To speed the atomistic calculations, we present results for the cutoff length $r_c = 1.5\sigma$, so that only nearest neighbors interact. There is no fundamental limit on the size of r_c, but the overlap region described below must be larger than r_c.

Substrate atoms are initially placed on the sites of a two-dimensional triangular lattice with the equilibrium nearest-neighbor spacing r_0 and a flat or rough surface (Figs. 1 and 2). Atoms in the top solid are fixed rigidly in the desired geometry, which is described for each example in Sec. III. They interact with substrate atoms through a purely repulsive potential obtained by truncating the LJ potential at $2^{1/6}\sigma$. The atomistic equations of motion are integrated with a velocity-Verlet algorithm using the large-scale atomic/molecular massively parallel simulator (LAMMPS) [30,31]. The time step $\Delta t_{MD} = 0.005\tau$, where $\tau \equiv \sqrt{m\sigma^2/\epsilon}$ and m is the mass of an atom.

Thermal fluctuations complicate the quantitative comparison between different simulations. They can be eliminated by long time averaging of steady-state quantities, but are harder to remove for dynamic simulations such as those described in Sec. III B. To maximize the precision of quantitative tests, we focus on a low temperature of $T = 0.0001\epsilon/k_B$, where k_B is Boltzmann's constant. We have also tested the method at $T = 0.1\epsilon/k_B$. For the purpose of testing the hybrid method, the same thermostat must be applied in both atomistic and continuum regions. The most convenient choice within LAMMPS is the Langevin thermostat [32], and we used a damp-

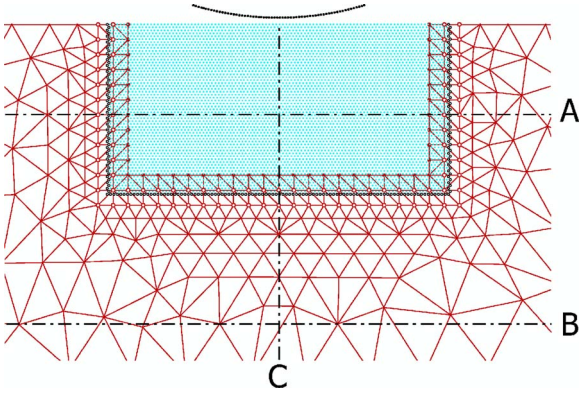

FIG. 2. (Color online) Geometry of the hybrid model near the contact between a rigid cylinder (top arc of black circles) and a deformable substrate (light blue circles). The total FEM region has a size of $400\sigma \times 200\sigma$ and extends outside the figure. Solid lines indicate the boundaries of elements and the smallest have edge 4σ. The atomistic region is about 1/16th of the total area, and atoms are indicated by circles. Stresses along lines *A* (depth of 30σ), *B* (depth of 100σ), and *C* (vertical center) are compared with results from pure MD simulations in Figs. 4 and 5.

ing rate of $0.1\tau^{-1}$ unless otherwise noted. More physically realistic thermostats that conserve local momentum could also be used [33].

The surfaces are brought together by rigid translation of the top solid. In some cases the height of the top solid is then fixed. In others a fixed external force is applied and the equations of motion of the top solid are followed [34,35]. In the latter case, the mass M of the top solid is the number of atoms it contains times m. Both normal forces (loads) and lateral forces (friction) are considered. The local stress within the solid is determined from the kinetic energy and virial terms as described in Ref. [36]. Atoms from the upper and lower solids are considered to be in contact whenever they are close enough to repel each other, $r < 2^{1/6}\sigma$.

B. Continuum description

In the hybrid method a continuum description is used in the region far below the surface where physical quantities change slowly. We use a finite-element mesh with linear, triangular elements, but the method could also be applied with higher-order elements. Unlike most methods, the mesh is not refined to the atomic separation near the overlap region. Indeed there need be no correlation between atomic and nodal positions. This may represent a major simplification, particularly in three dimensions where meshing or remeshing to specific nodal positions is difficult.

There are two other reasons why we do not refine the mesh to atomic scales. One is that when the mesh dimension is smaller than the interaction range, the energy of the element depends on displacements of surrounding nodes. This nonlocal effect is included in FEAt [15], but complicates the finite-element code. A second is that at finite temperatures the constitutive law is a function of scale. This scale dependence is captured approximately by the finite-T formulation of QCM [9] and in methods that integrate out fine scale degrees of freedom [10,11]. Applying a bulk constitutive law at the atomic scale can lead to significant errors at high temperatures.

As in the atomistic simulations, periodic boundary conditions are applied along the interface (x direction) and the bottom nodes in the mesh are fixed. In most cases the mesh coarsens with depth as stress gradients decrease (Figs. 1 and 2). An explicit dynamic FEM algorithm is used [37]. The trajectories of nodes are integrated with the second-order Newmark method. The time step Δt_{FE} is small enough to satisfy the stability requirement for the smallest element and is described further in the next subsection. A Langevin thermostat with the same damping rate used in atomistic simulations is added to the equations for each node. Note that specifying the rate, rather than a drag coefficient, ensures that the damping of a wave is independent of the mesh size.

A linear constitutive law is not adequate for the contact problems of interest here. Nonlinear effects become significant at strains of about 0.3%, and compressive strains remain above this level far below the surface (Sec. III A 1). Since the overlap region must be placed at a depth where the constitutive law is accurate, a large fraction of the system must be treated atomistically if a linear law is used. We use a simple quadratic constitutive law here, but the approach is readily extended to more complicated laws. One could also implement an algorithm where stresses are interpolated from a table, with new values calculated as needed. Note that the QCM avoids the need for a constitutive law by calculating the energy exactly for an affine deformation of atoms in an element. However, this is only straightforward at zero temperature where the energy rather than the free energy controls the stress and for periodic crystalline substrates. Approximate treatments of the entropic contribution to the stress have recently been proposed [9], but require more computation. In addition, the approximate nature of the stress calculation means that it does not yield the correct lattice constant and elastic moduli, so that simple constitutive laws may be more accurate.

To determine the constitutive law, one can evaluate the stress as a function of strain for a small crystal with periodic boundary conditions. The number of strains that must be considered depends on the symmetry of the system, but in general much less simulation time is required than for any other part of the calculation. The equilibrium density is determined from zero-pressure simulations at the temperature of interest, and the constitutive relation is expressed as a function of the strain relative to this reference state. Including all quadratic terms allowed by symmetry in a two-dimensional (2D) system gives

$$\sigma_{xx} = c_{11}u_{x,x}(1 + \alpha_1 u_{x,x}) + c_{12}u_{y,y}(1 + \alpha_2 u_{y,y}) + \alpha_3 u_{x,y}^2 + \alpha_4 u_{y,x}^2 + \alpha_5 u_{x,x}u_{y,y} + \alpha_6 u_{x,y}u_{y,x},$$

$$\sigma_{yy} = c_{22}u_{y,y}(1 + \beta_1 u_{y,y}) + c_{12}u_{x,x}(1 + \beta_2 u_{x,x}) + \beta_3 u_{x,y}^2 + \beta_4 u_{y,x}^2 + \beta_5 u_{x,x}u_{y,y} + \beta_6 u_{x,y}u_{y,x},$$

$$\sigma_{xy} = \sigma_{yx} = c_{33}(u_{x,y} + u_{y,x})/2 + \gamma_1 u_{x,y}u_{y,x}, \quad (2)$$

where $u_{i,j} \equiv \partial u_i / \partial x_j$, u_i is the displacement along coordinate i, and x_j is the initial position of the atom along coordinate j. Note that using the nonlinear Lagrangian strain tensor $(u_{i,j} + u_{j,i} + u_{k,i}u_{k,j})/2$ at lowest order does not yield all of the terms for the diagonal stress components in Eq. (2). However, it does yield the quadratic term for the off-diagonal stress and with ratios of coefficients that are nearly consistent with those determined below.

The triangular lattice is isotropic at the linear level, implying $c_{11}=c_{22}$ and $c_{33}=c_{12}$. The Poisson ratio $\nu \equiv c_{12}/c_{11} = 1/3$, leaving a single parameter to be determined. Fits for small displacements give $c_{12}=c_{33}=c_{11}/3=25.14\epsilon\sigma^{-2}$. The quadratic terms in the expansion are not isotropic, but are related by sixfold symmetry. They were determined individually by changing individual or pairs of strains to minimize cross talk. The measured stress was fit to better than 0.5% up to strains of 2% with the parameters: $\alpha_1=10.0$, $\alpha_2=9.8$, $\alpha_3 = 12.3\epsilon\sigma^{-2}$, $\alpha_4=38\epsilon\sigma^{-2}$, $\alpha_5=200\epsilon\sigma^{-2}$, $\alpha_6=100\epsilon\sigma^{-2}$, $\beta_1=7.4$, $\beta_2=2.9$, $\beta_3=186\epsilon\sigma^{-2}$, $\beta_4=163\epsilon\sigma^{-2}$, $\beta_5=550\epsilon\sigma^{-2}$, $\beta_6 = 413\epsilon\sigma^{-2}$, and $\gamma_1=45\epsilon\sigma^{-2}$.

We will compare our results to classical continuum contact mechanics for ideally elastic and isotropic materials. There the only constitutive parameter is an effective modulus $E^* \equiv E/(1-\nu^2)$, where $E \equiv c_{11} - c_{12}/\nu = c_{11}(1-\nu^2)$ is Young's modulus [1]. For our system, $E^*=75.42\epsilon\sigma^{-2}$ at zero strain. In anisotropic crystalline materials, E depends on the orientation of the surface. Studies of such materials show that the standard continuum equations can be used, but the value of E^* must be determined numerically for each orientation [1].

C. Coupling scheme

We use an overlap region to connect MD and FEM regions and pass local deformations in both directions. As shown in Fig. 1, top nodes of the mesh follow the displacement of the atoms around them, while atoms on the bottom boundary of the MD region get displacement information from the mesh element that they belong to. There is some freedom in the exact procedure for determining the displacements that are passed between descriptions. The differences between them are qualitatively similar to the differences between different order elements or different choices of mesh size in FEM methods [19].

For the results shown below, each atom on the MD boundary (small open circles) is associated with the mesh element containing its initial atomic position. The displacement of the atom is then interpolated from the nodal displacements using the initial position and the shape functions for the element [38]. As noted above, linear elements are used. In order to provide complete boundary conditions for the atomistic region, the width of the region of interpolated atoms must exceed the interaction range r_c. Only a single atom is required here, since we use nearest-neighbor interactions. For very long-range interactions it may be possible to use a small overlap region and replace the outer atoms by a spatial integral [32]. However, representing constitutive relations on mesh elements smaller than r_c is not generally accurate. This is why the computationally expensive nonlocal version of the QCM must be applied in the regions that are refined to atomic scales. The transition from nonlocal to local schemes as the mesh coarsens then introduces complicated ghost forces. Using an overlap region that is wider than r_c ensures that no ghost forces enter the dynamics in the purely atomistic region of our system.

The positions of the boundary nodes (large solid circles) of the mesh were determined by averaging the displacements of all atoms whose initial position is nearby. One approach is to invert the relation connecting nodal and local displacements. Each node is then affected by all atoms whose initial positions lie inside the elements that contain the node. For our example, this corresponds to atoms in a deformed hexagonal region. This approach has the disadvantage that only half the mesh elements associated with boundary nodes are defined and the weighting function is complex (although it is only calculated once). A simpler approach is to replace the averaging area by a circle of comparable area (dotted circle) and use a weighting function consistent with the FEM. Since we use linear elements, we use a weight that decreases linearly with distance and reaches zero at a radius r_{av}. In most cases, $r_{av}=4\sigma$, which is comparable to the separation between nodes $(4\text{-}5\sigma)$. Smaller radii and uniform weighting functions were also tried. As long as the gradient in strain is small, the results are not significantly different.

The coupling methods of FEAt and CADD can be viewed as specific limits of the above in which the mesh is refined to atomic scales and nodes coincide with atoms. In these methods the atoms whose displacements follow nodes (small open circles) are directly adjacent to atoms that determine displacements of boundary nodes (large solid circles). In our generalized approach, they may be separated by several layers of unconstrained atoms. In fluid applications [18,19,39] this played an important role in allowing perturbations produced by the atomic boundary to equilibrate before affecting the motion of the atoms that determined continuum displacements. A similar equilibration of fluctuations about crystalline lattice sites may be important in solids at higher temperatures.

Our multiscale method uses different time as well as different spatial scales. The time step in atomistic regions, Δt_{MD}, must be small enough to resolve the rapid motion of individual atoms. Since each node corresponds to multiple atoms, a larger time step Δt_{FE} can be used for their dynamics. In principle the time step could coarsen with mesh size, but the FEM portion of the calculation was so fast that a single Δt_{FE} corresponding to the smallest elements was used. For the results shown, the smallest nodal separation is about 4 times the atomic separation and $\Delta t_{FE}=20\Delta t_{MD}$. This is about 1/4 of the maximum stable time step for the FEM, which corresponds to the time for sound to propagate across the smallest circle that fits into an element.

The different time scales of the FEM and atomistic descriptions mean that displacements in the overlap region must be extrapolated and interpolated. We followed an interleaving procedure that was successful in a similar method for fluid dynamics [18]. Nodal positions at the boundary of the FEM for time $t_n=n\Delta t_{FE}$ are determined by averaging the atomic displacements within r_{av} from $t_n-0.5\Delta t_{FE}$ to $t_n + 0.5\Delta t_{FE}$. The FEM code is then called to advance all other nodal positions to t_n. Extrapolated values of the nodal posi-

tions that determine atomic displacements on the boundary are also obtained for $t_n+0.5\Delta t_{FE}$ to $t_n+1.5\Delta t_{FE}$. The MD simulation can then be run for this next time interval and the process repeated. Choosing Δt_{FE} below the stability limit guarantees that nodal displacements are small enough that the linear extrapolation is reasonable. To confirm this, we checked that there was little dependence on the ratio $\Delta t_{FE}/\Delta t_{MD}$ as it was reduced to unity. Extrapolating the atomic positions would be less stable, because of their more rapid changes.

III. RESULTS

A. Steady-state simulations

1. Single-asperity contacts

Contact between a cylinder and a flat substrate is one of the classic problems in continuum contact mechanics. Within the continuum description [1], the general case of two elastic bodies can be reduced to a rigid cylinder and an elastic substrate with an effective modulus E^*. We consider this simpler case, with a tip radius $R=100\sigma$ that would be typical of an atomic force microscope tip [5,40]. The CADD method [41] has been used to study nanoindentation by an idealized smooth cylinder at larger loads than those considered here. Full MD simulations [5] indicate that the specific atomic structure of the cylindrical tip may play an important role, and we consider the simplest geometry used there, a bent crystalline tip.

One key quantity is the size of the contacting region, which is normally expressed as $2a$, where a is the half-width. In continuum theory for ideal elastic solids

$$a = \sqrt{4NR/\pi E^*}, \tag{3}$$

where the normal load N pushing the surfaces together must be small enough that $a \ll R$. The subsurface stress is also important because it determines the onset of plastic deformation. Yield is usually assumed to initiate where the deviatoric shear stress is largest, which is predicted to occur at a depth of $0.78a$ below the surface [1].

Figure 2 shows the geometry of the mesh and atomistic region for the hybrid method. An atomistic description is only important in the region near the contact where stresses and strains are largest. However, subsurface deformations are important in determining the size of the contact due to the long-range nature of elastic deformations. To minimize boundary effects, the depth D and lateral period L must be much greater than a. In a previous paper [5], we used an all atomistic description with $L=400\sigma$ and $D=200\sigma$ to approach this limit. For our hybrid calculation we use the same geometry, but only treat $1/16$ of the area atomistically. A gradually coarsening FEM is used in the remainder of the area.

The tip is represented by a crystal bent into a circular arc. Since the tip-substrate interaction is purely repulsive and short range (Sec. II A), a single layer of surface atoms on the cylinder is sufficient. We consider two values of the atomic spacing r_0' in the tip. To approach the limit of continuum theory we use a dense tip with atoms spaced by a tenth of the atomic spacing r_0 in the substrate. To reveal effects of atomic discreteness we consider $r_0'=r_0$, allowing the atoms to lock together easily. We will refer to this as the commensurate tip. All substrate atoms that are close enough to be repelled by the tip are considered to be part of the contact.

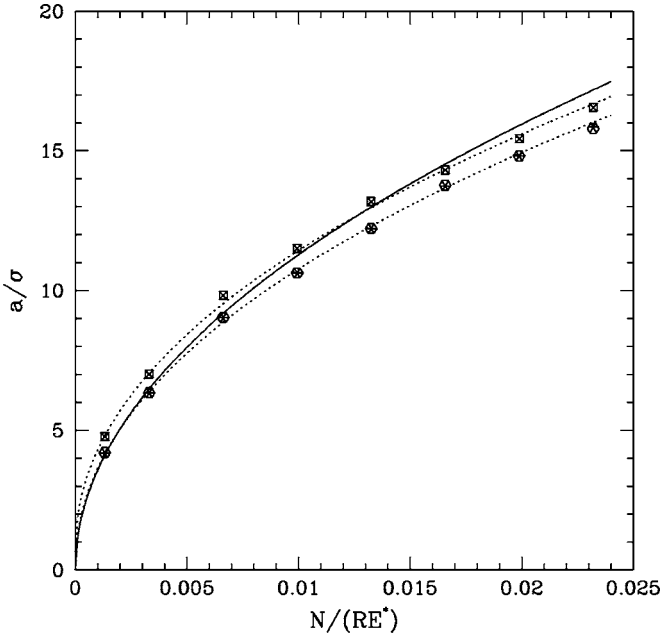

FIG. 3. Relation between contact radius a and load N for 2D cylindrical contact. Open hexagons and squares show all atomistic results for dense and commensurate cylinders, respectively. The corresponding hybrid results are indicated by asterices and crosses. A solid line shows the continuum prediction for elastic solids and dotted lines are guides to the eye.

Figure 3 shows the contact half-width a as a function of N for dense and commensurate tips. In both cases, results from the hybrid method and fully atomistic calculations are indistinguishable over the entire range of loads. Previous simulations [5] with the dense tip that used purely linear elastic interactions between substrate atoms were in good agreement with the continuum prediction given by Eq. (3) (solid line). This agreement is also seen at small loads in Fig. 3. As the load increases, the nonlinearity of the LJ interactions used here grows in importance, leading to a monotonic increase in the deviation from continuum theory. The LJ bonds stiffen with increasing strain, reducing the deformation and thus decreasing the size of the contact region relative to the elastic prediction. Increasing the load beyond the values shown produces plastic deformation, which is discussed further in the next subsection and Ref. [4].

Results for the commensurate tip are consistently higher than those for the dense tip. As discussed in Refs. [5,6], atomic structure makes tips appear rougher and smears the contact region. Even larger effects are observed for other atomic approximations to cylindrical or spherical tips, such as amorphous or stepped surfaces [5,6]. Similar effects may be important for macroscopic rough surfaces because statistical analyses of their contacts indicate that most are at very small scales [2,3]. This effect is considered in the next subsection.

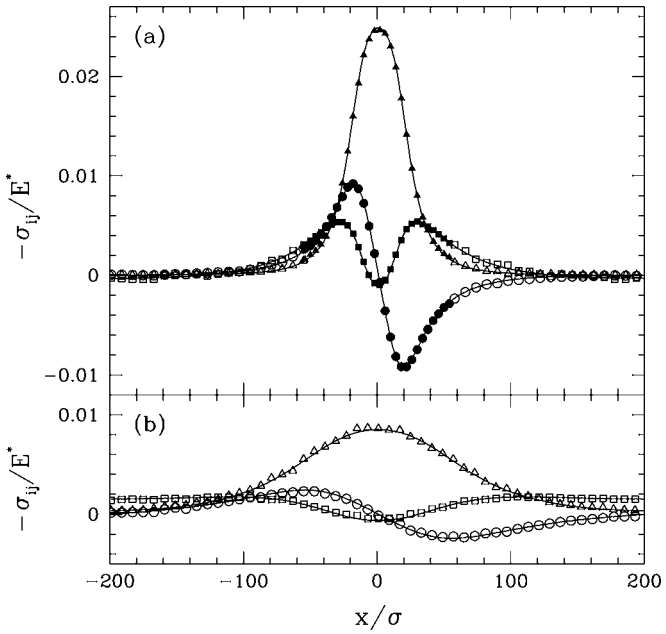

FIG. 4. Stresses normalized by E^* as a function of lateral position at depths of (a) 30σ and (b) 100σ below the surface that are indicated by lines *A* and *B* in Fig. 2, respectively. Hybrid results for σ_{yy} (triangles), σ_{xy} (squares), and σ_{xx} (circles) are compared to pure atomistic simulations (solid lines). In (a) there is a smooth transition between atomistic values (solid symbols) and FEM values (open symbols) in the overlap region. Here $N/RE^*=0.0132$ and the minus sign is introduced so that positive values correspond to compressive stresses.

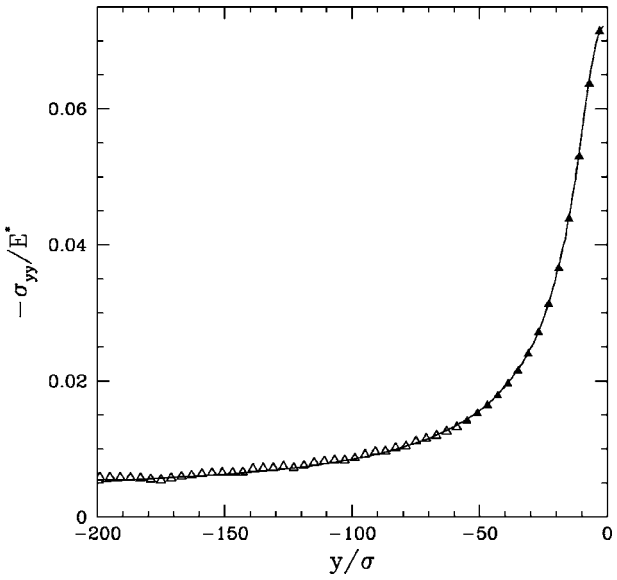

FIG. 5. Normalized stress σ_{yy}/E^* as a function of depth y below the center of the substrate (line *C* in Fig. 2). A solid line shows the stress from a purely atomistic simulation, and solid and open triangles show stresses in the MD and FEM regions of the hybrid calculation, respectively. Here $N/RE^*=0.0132$ and the minus sign is introduced so that positive values correspond to compressive stresses.

Figures 4 and 5 compare the subsurface stresses calculated from the hybrid method and pure atomistic simulations at $N/RE^*=0.0132$. The stresses are normalized by E^* so that values for σ_{yy} correspond roughly to the compressive strain, and values for σ_{xx} and σ_{xy} are roughly one-third of the corresponding strains. Stresses in FEM regions (open symbols) are linearly interpolated from the stresses on nearby Gaussian points. Stresses in the MD region are calculated from the local microscopic stress tensor [32]. In all cases, results from the two methods are nearly indistinguishable in the plot. An analysis for the root-mean-square (rms) deviations shows that they are about $10^{-4}E^*$ in Fig. 4 and $3\times10^{-4}E^*$ in Fig. 5. In all cases, this is less than 1% of the peak values.

Figure 4 shows the stresses along lines *A* and *B* in Fig. 2, corresponding to depths of 30σ and 100σ below the undeformed surface, respectively. Figure 5 shows the normal stress σ_{yy} along line C in Fig. 2. Note that along lines that pass through the overlap region (*A* and *C*) the stresses from the atomistic and FEM regions of the hybrid method are continuous. The constraints on the displacements in the overlap region ensure continuity of the strain tensor, but the stress tensor is only continuous if the constitutive relation is accurate for strains in the overlap region. This condition determines how large the atomistic region must be. When a purely linear constitutive law was used in the continuum we observed a discrepancy of 10% between continuum and atomistic stresses in the overlap region. This led to similar discrepancies between the total force applied to the top surface and that transmitted to the bottom of the substrate.

Along line *A* (Fig. 4) the stresses correspond to strains of up to 2.5%, while our quadratic constitutive model is only fit to 2% strains. Even 100σ below the surface (line *B*) the strains ($\sim$1%) are 3 times larger than can be accurately described by linear elasticity. From Fig. 5 we see that the compressive stress remains above 2% until depths of about 35σ for this load. The overlap region must be below this depth. Fitting the constitutive relation to larger strains would relax this condition. However, another constraint is that the change in strain over the mesh size in the overlap region must be small enough for the linear elements to be accurate. This constraint and dynamic constraints are discussed in Sec. III B.

For the purpose of illustrating the method we have chosen a fixed overlap region with a simple rectangular geometry that is large enough to be accurate at the largest loads. A more efficient approach would be to determine the overlap region dynamically. The instantaneous values of local strain and strain derivatives determine where the constitutive relation is accurate. The atomistic region could be expanded into regions of growing strain and shrunk where the constitutive relations are accurate.

2. Contact between rough surfaces

The simple cylindrical geometry considered above is relatively easy to treat with analytic or single-scale numerical approaches. Real surfaces typically have roughness on many different length scales and thus pose a much greater computational challenge. A large interface must be treated to obtain

a statistical sampling of the roughness, and a roughly equal depth must be included in order to capture the effects of subsurface deformations. These deformations produce long-range correlations that qualitatively alter the contact geometry [2–4].

To test our method for more complex surfaces we consider contact between a rigid flat surface and a deformable substrate with a self-affine fractal surface [42]. Self-affine surfaces are characterized by a Hurst or roughness exponent H, which is between 0 and 1. The rms change in height $w(\ell)$ over a lateral distance ℓ scales as $w(\ell) \propto \ell^H$. At large ℓ the surface appears flat because w grows more slowly than ℓ. At small ℓ the mean surface slope diverges since $w/\ell \sim \ell^{-(1-H)}$. For any real surface, this divergence is cut off because the scaling cannot extend to lengths smaller than the interatomic spacing.

The deformable substrate had a lateral period of $L = 1024 r_0 = 1149\sigma$ and a depth $D = 972\sigma$. A self-affine curve with $H = 0.5$ was generated using the successive random midpoint algorithm of Voss [42]. The curve was resolved to $r_0/2$, since this is the lateral spacing between atoms on successive layers. The rms slope on this smallest scale was 0.26 and the mean height was zero. Then all atoms on a triangular lattice whose height lay above the surface were removed. A small piece of the resulting system is shown in Fig. 1. Purely atomistic simulations involved more than 10^6 atoms and $10^5 \Delta t_{MD}$, and strained the limits of our local computer cluster. In the hybrid method, the overlap region was placed at an average depth of 50σ below the surface, reducing the number of atoms (and the total computation time) by about a factor of 20. The smallest mesh elements had an edge length of 4σ.

The rigid flat surface has the same atomic spacing r_0 as the substrate. A constant load is applied and the system allowed to equilibrate. Rigid atoms that interact with the substrate are considered to be part of the total length L_c of molecular contact. The fraction L_c/L of the total period L along the interface that is in contact is just the fraction of rigid atoms that interact with the substrate.

Figure 6 shows the variation of L_c/L with the dimensionless load N/LE^*. As before, results from the hybrid and purely atomistic simulations are in excellent agreement. The small difference between the two points near $L_c/L = 0.09$ represents a stochastic fluctuation rather than a systematic error. Some jumps in the area result from plastic rearrangements where atoms on the top layer of a peak in the substrate are pushed down into the next layer [4]. This is a nucleated event that is very sensitive to the loading history and small oscillations of the top surface under the constant load. The hybrid simulation followed the same sequence of events, but at slightly shifted times. Similar variations were observed between different atomistic simulations for the same geometry and different initial velocities. For the loads considered here, plastic deformation was confined to the inner portion of the atomistic region. The atomistic region would need to be extended if dislocations propagated to the overlap region. Alternatively, discrete dislocations could be included in the continuum model [20].

Continuum calculations and simulations generally predict a linear relation between L_c and N. Our numerical results are

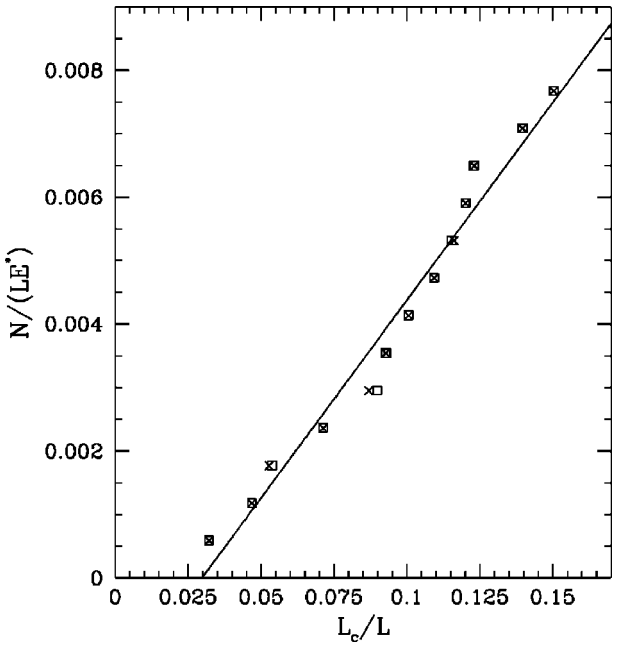

FIG. 6. Variation of the fraction of interface length in contact L_c/L with dimensionless normal load $N/(LE^*)$ from purely atomistic simulations (squares) and the hybrid method (crosses). The substrate had a lateral period $L = 1024 r_0$ and a self-affine topography with $H = 0.5$ and rms slope 0.26 at the smallest scale.

roughly consistent with a linear fit, but L_c/L goes to a constant at small loads. The reason is that the surface height can only change in discrete steps of the spacing between atomic layers, $3^{1/2} r_0/2$. For this L, a significant fraction of the substrate has the same height and contacts the top surface at the same time. As L increases, this effect decreases, but the slope remains much smaller than predicted by continuum calculations [4].

B. Dynamic simulations

The above simulations show that the hybrid method provides an accurate description of steady state properties. A more stringent test of the method is the response to time varying strains. One potential source of error is the interpolation and extrapolation over Δt_{FE} to match the time scales of the atomistic and FEM regions. Another concern is whether the overlap region leads to spurious reflections of lattice vibrations.

The problems of main interest to us involve contact and friction at interfaces. The interface is then the main source of vibrations. We consider two test cases: pulses driven by displacing the top of the substrate and friction between rough surfaces.

1. Pulse propagation

Pulse propagation through a deformable substrate was studied for a system of width $L = 64 r_0 = 71.8\sigma$ and $D = 200\sigma$. In the hybrid model the region $y > -96.2\sigma$ was treated atomistically. A uniform triangular mesh with nodal spacing 4σ was used for $y < -89.8\sigma$. The coarser spacing in the FEM

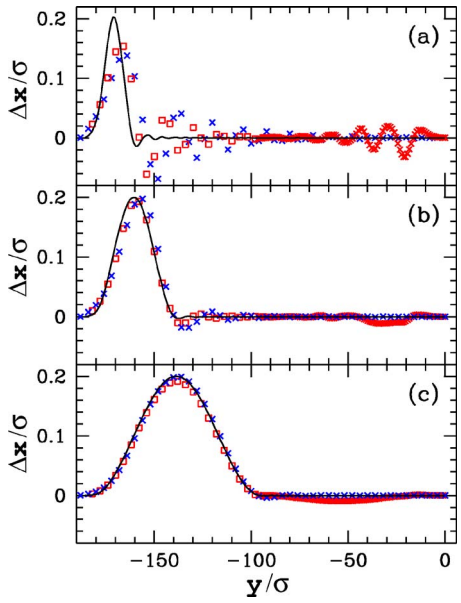

FIG. 7. (Color online) Shear displacement Δx as a function of depth below the surface for fully atomistic calculations (solid lines), FEM calculations with a constant mesh-size (blue crosses), and the hybrid method (red squares). The pulse is initiated at the surface ($y=0$), and all results are for the time where the leading edge of the pulse reaches the bottom of the atomistic system. The full width at half maximum is (a) 11σ, (b) 22σ, and (c) 44σ and the nodal spacing on the FEM is about 4σ.

region means that short-wavelength modes can not propagate from the atomistic region and will be reflected. Similar problems are well known in pure FEM calculations with a coarsening mesh [38]. To separate errors produced by the coarse FEM mesh from those intrinsic to the hybrid method, we also present purely FEM results with a constant mesh size equal to that in the continuum portion of the hybrid method.

The entire flat top layer was displaced laterally to generate a shear pulse. The form of the displacement was $\Delta x=0.1[1-\cos(\omega t)]\sigma$ for $0<t<2\pi/\omega$ and zero for earlier and later times. This generates a pulse with full width at half the maximum of about $\Delta y=c_s\pi/\omega$, where $c_s=4.9\sigma/\tau$ is the shear velocity. Pulse widths of about 11σ, 22σ, and 44σ are shown, corresponding to about 3, 5.5, and 11 times the FEM mesh size. The peak strains are small enough to be described by the constitutive relations. For these simulations the thermostat was turned off to eliminate damping during transmission.

Figure 7 shows the mean shear displacement along x as a function of depth at the time when the leading edge of the pulse is reaching the bottom of the fully atomistic system. The hybrid method and pure FEM calculation are close to the purely atomistic results for the largest pulse width [Fig. 7(c)]. Both methods show increasing deviations from atomistic results as the pulse width decreases. The similarity between the changes in pulse shape shows that the coarseness of the FEM mesh is the main source of error. The propagation velocity on the coarse mesh is too slow, causing the pulses to lag behind the atomistic results. Oscillations also appear at the tail of the pulses because the frequency-dependent dispersion relation is altered. Note that both of these changes are more noticeable for the pure FEM results. This is because the pulse travels on the coarse mesh over the entire FEM system, while the coarse mesh starts in the overlap region for the hybrid system.

The resolution change in the overlap region leads to an additional reflected wave in the hybrid results. A similar effect would be observed in a pure FEM calculation with a sudden change in mesh size. The magnitude of the reflected wave was quantified by taking the ratio between the energy carried in the reflected wave to the total energy in the original wave. As the pulse width increases from Figs. 7(a)–7(c), the percentage reflected decreases from 21.6% to 1.1% to 0.31%. For most purposes using a mesh size of 1/10 the pulse width appears to be adequate.

A number of methods for minimizing reflections have been explored for linear systems. The work of Cai *et al.* [24] can in principle be used at any temperature, but involves simulating the full geometry atomistically before doing multiscale simulations. E and Huang [25] have developed a local method capable of reducing reflections in linear systems at $T=0$. Both approaches deal with reflection at a sharp interface, and not the effects of the gradual coarsening in efficient FEM meshes. Algorithms that can overcome these limitations and address nonlinearity are an important topic for future research, but at present we restrict attention to regimes where reflections are not important.

We have explored the effect of parameters in our coupling scheme on the magnitude of reflected waves. One is the radius r_{av} of the circle over which atomic displacements are averaged to fix nodal displacements. Decreasing r_{av} from 4σ to 1σ reduced reflections to 15.3%, 0.56%, and 0.085% for the three widths in Fig. 7. However, it seems most natural for r_{av} to correspond to the area represented by each node. This became more important when the temperature was increased, because the thermal fluctuations of atoms in a smaller region are larger than those appropriate for the nodal points.

As noted above, no thermostat was applied during these pulse simulations. The hybrid method remained stable over this interval ($\sim 40\tau$). When the simulation time was extended by more than an order of magnitude ($\sim 500\tau$), changes in the energy became significant and the temperature grew continuously. Analysis of one-dimensional analogs of our system indicates that the coupling in the overlap region may introduce a weak, small-wavelength instability. A similar temperature rise occurs in purely atomistic simulations when a Gear predictor-corrector algorithm is used without a thermostat [32]. As there, our hybrid simulations remain stable and produce results that are statistically equivalent to other methods as long as the system is coupled to a thermal bath on a time scale shorter than the time for temperature growth.

2. Friction on rough surfaces

In problems involving contact and friction between rough surfaces, the dominant wavelength of the elastic deformations that couple asperities will scale with the depth below the surface. Using standard criteria for mesh quality will ensure that the mesh size is much smaller than the depth in order to capture these deformations. The pulse results shown

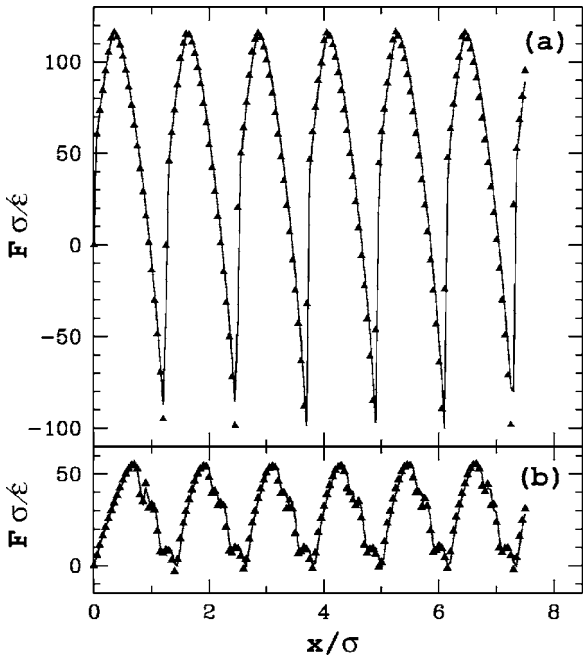

FIG. 8. Friction F as a function of the lateral displacement of the top wall at $v=0.01\sigma/\tau$ and load $N=204.8\epsilon/\sigma$. Hybrid results (symbols) and pure atomistic simulations (lines) are shown for (a) a flat substrate and (b) the self-affine surface of Sec. III A 2.

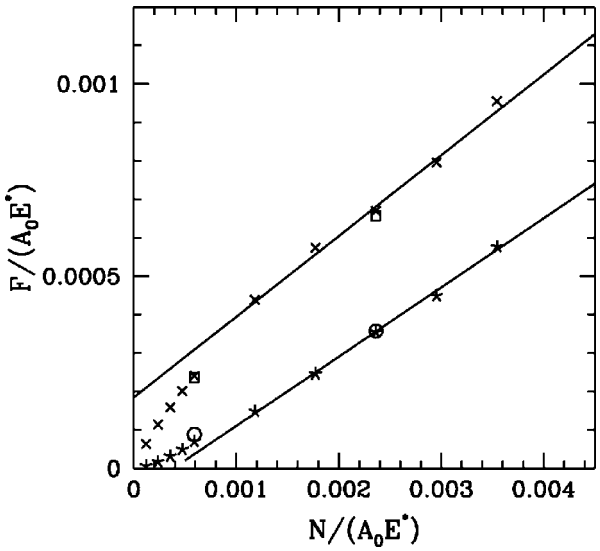

FIG. 9. Friction as a function of load for the rough surface of Sec. III A 2. The static friction from hybrid and fully atomistic simulations is shown by crosses and squares, respectively. The corresponding kinetic friction is indicated by asterisks and circles.

in the previous subsection place similar constraints on the mesh. They indicate that for the dynamic changes in the elastic deformations to propagate smoothly, the mesh size should be less than 10% of the depth.

To test the hybrid method in simulations of sliding friction, we consider a flat rigid crystal sliding over a flat or rough deformable substrate. The rough surface has the same self-affine topography considered in Sec. III A 2. In both cases the mesh size in the overlap region, 4σ, is less than 10% of the depth of the atomistic region, 50σ.

The flat, upper solid is moved laterally at a constant velocity of $v_x=0.01\sigma/\tau$, while a constant normal load N is applied. Figure 8 shows the friction force as a function of sliding distance for $N=204.8\epsilon/\sigma$. Results from the hybrid method (points) accurately reproduce those from purely atomistic simulations.

In these simulations, the rigid and deformable solids have the same lattice constant r_0. The friction force varies periodically as the top solid is advanced by one lattice constant. For the flat surface all top atoms move coherently up and down over the substrate atoms and the resulting friction is large. For the rough surface, only about 7.2% of the surface is in contact at this load. The contacting region is broken up into many small regions where local peaks hit the top wall. The sum of the peak forces for each region is comparable to that for the flat surface, but the peaks advance out of phase, reducing the amplitude of the periodic force. Two factors contribute to the dephasing. One is a Poisson ratio effect. Pressure on a peak causes a lateral expansion of the surrounding material. Even though periodic boundary conditions are imposed, fluctuations in pressure lead to fluctuations in the lateral spacing of peaks. A more important effect is that alternate layers of the triangular lattice are shifted laterally by $r_0/2$. Peaks whose highest points are on odd and even layers will tend to advance exactly out of phase. The total force does not cancel because of Poisson effects and because a small number of contacts provide most of the force.

At the velocity considered here, the temporal period of the force is $r_0/v\approx 112\tau$. This is about 7 times longer than the longest pulse in Fig. 7. Studies at higher velocities show that the hybrid method continues to reproduce atomistic results. However, in many cases the quantity of interest is the kinetic friction in the quasistatic limit. This requires that stress can equilibrate on the scale L_m of the largest wavelength of lateral roughness and over a depth of the same scale. The time for stress equilibration is of order L_m/c_s, and this should be less than the time scale for changes in the surface force r_0/v. One concludes that to be in the quasistatic limit one must have $v \ll c_s r_0/L_m$. For a typical atomic force microscope experiment $L_m\sim 10$ nm and $v\sim 1$ mm/s $\ll c_s r_0/L_M\sim 30$ m/s, using $r_0\sim 0.3$ nm and $c_s\sim 10^3$ m/s. Similarly, for a surface force apparatus, $L_m\sim 100$ μm and $v\sim 1$ μm/s $\ll c_s r_0/L_M \sim 3$ mm/s. For the simulations shown in Fig. 8, $v \approx 2c_s r_0/L_m$, so stress only equilibrates over half the system depth. As noted above, reflections would not become important until the velocity increased by more than an order of magnitude, and the method becomes more accurate as the velocity decreases into the quasistatic regime. We conclude that the approach can be used over a wide range of velocities from the quasistatic limit to a few percent of the sound velocity.

Experiments typically identify two types of friction: the static friction F_s needed to initiate sliding and the kinetic friction F_k needed to maintain steady sliding at a velocity v. The peak force corresponds to F_s. Values of F_k were obtained by averaging curves like those in Fig. 8 over a distance of 15σ. Both quantities are plotted as a function of normal load in Fig. 9. Once again, results from the hybrid method are in

excellent agreement with purely atomistic simulations, while requiring a small fraction of the computational effort. Indeed the purely atomistic simulations were so computationally intensive that values were only obtained for two loads. The hybrid method allowed us to explore the effect of load in full detail.

At small loads, the real contact area L_c is constant. This corresponds to the area in the limit of zero load in Fig. 6. In this limit the static friction force increases linearly with the load, because the potential energy barrier for displacing each atom rises linearly with load [43]. The kinetic friction rises much more slowly, because the positive and negative forces produced by the potential nearly cancel [44]. Both frictions rise with a different slope for $N/(LE^*) > 0.0006$ where L_c rises linearly with load (Fig. 6). The static friction rises more slowly than at low loads because contributions to the total force from the increased area do not all add in phase. The kinetic friction rises more rapidly because the regions of negative force are suppressed. This is related to an increase in the ratio of interfacial stiffness to bulk stiffness with increasing load [44,45].

IV. SUMMARY AND CONCLUSIONS

We have implemented a hybrid method that treats interfacial effects atomistically, while capturing long-range elastic deformations using continuum FEM techniques. To avoid discontinuous transitions in behavior, the atomistic and continuum descriptions are coupled via an overlap region that is wider than the interaction range. At the outer boundaries of the overlap region, displacements from one description provide boundary conditions for the other (Fig. 1). The FEM need not be refined to atomic scales, and there is no need to constrain nodal positions to coincide with atoms. The hybrid method can be applied to quasistatic or dynamic problems at any temperature where the solid remains stable, as long as the appropriate temperature-dependent constitutive law is used.

The method was tested by comparing to purely atomistic simulations of quasistatic and dynamic processes in simple and complex rough geometries. A low temperature was used to allow precision comparisons and to minimize stochastic differences in dynamic quantities. Quasistatic results for the contact area (Figs. 3 and 6) and subsurface stress (Figs. 4 and 5) were extremely accurate when the correct nonlinear constitutive relation was used. The hybrid method also reproduced atomistic results for the time dependence of friction forces (Fig. 8) and allowed us to calculate the static and kinetic friction over a much wider range of loads than was feasible with purely atomistic simulations (Fig. 9).

Studies of pulse propagation illustrate the potential limitations of the method for dynamic simulations (Fig. 7). Pulses moving from the atomistic to FEM region suffered distortion and reflection when the pulse width was comparable to the FEM resolution (Fig. 7). These effects are not intrinsic to the hybrid method and are also encountered in any FEM calculation when the mesh size coarsens. Recent algorithms reduce reflections at the boundaries of atomistic regions [24,25], but transmission of crucial low-frequency strain waves may also be affected and they remain limited to linear constitutive laws. Development of general, nonlinear, finite-temperature methods for minimizing reflections from atomistic boundaries and changes in mesh size remains an important issue for future research.

The velocities of interest in friction simulations are often low enough to be in the quasistatic limit where the dominant wavelengths exceed not only size of the largest mesh elements but the entire system size. Shorter-wavelength vibrations generated by atomic collisions, local stick-slip motion, and other rapid processes are important mainly as channels of energy dissipation. In experimental systems these rapid vibrations would be converted to heat by viscoelastic damping in the solid or incoherent scattering at boundaries or impurities. Except in extremely small systems and at high velocities, coherent reflections from boundaries do not appear to play an important role in the dynamics. Given this, the key goals of any simulation method should be to limit spurious reflections at artificial boundaries like the overlap region and minimize reflections at real boundaries by damping waves or ensuring that scattering is incoherent. In the simulations described here, damping was implemented using a Langevin thermostat. This violates momentum conservation and a more physical approach would be to use a viscoelastic constitutive law for the FEM region and a corresponding diffusive particle dynamics in the atomistic region [33].

Although the method has only been applied to 2D problems here, it is straightforward to extend it to 3D systems. A more ambitious goal is to implement dynamic remeshing algorithms that expand or shrink the atomistic region in response to changing stresses. Work on both extensions is currently underway.

ACKNOWLEDGMENTS

This paper is based on work supported by the National Science Foundation under Grant Nos. CMS-0103408, CTS-0320907, and DMR-0454947. The work of N.B. was supported by the U.S. Office of Naval Research and the Naval Research Laboratory. We thank S. Chen, W. E., J. A. Harrison, R. E. Miller, and L. Pei for useful discussions.

[1] K. L. Johnson, *Contact Mechanics* (Cambridge University Press, New York, 1985).

[2] S. Hyun, L. Pei, J.-F. Molinari, and M. O. Robbins, Phys. Rev. E **70**, 026117 (2004).

[3] L. Pei, S. Hyun, J.-F. Molinari, and M. O. Robbins, J. Mech. Phys. Solids **53**, 2385 (2005).

[4] B. Q. Luan, S. Hyun, M. O. Robbins, and N. Bernstein, in *Fundamentals of Nanoindentation and Nanotribology*, edited

by K. J. Wahl, N. Huber, A. B. Mann, D. F. Bahr, and Y.-T. Cheng, MRS Symposia Proceedings No. 841 (Materials Research Society, Warrendale, PA, 2005), p. R7.4.
[5] B. Q. Luan and M. O. Robbins, Nature (London) **435**, 929 (2005); Phys. Rev. E **74**, 026111 (2006).
[6] B. Luan, Ph.D. thesis, Johns Hopkins University, Baltimore, 2006.
[7] E. B. Tadmor, M. Ortiz, and R. Phillips, Philos. Mag. A **73**, 1529 (1996).
[8] V. B. Shenoy, R. Miller, E. B. Tadmor, R. Phillips, and M. Ortiz, Phys. Rev. Lett. **80**, 742 (1998).
[9] L. M. Dupuy, E. B. Tadmor, R. E. Miller, and R. Phillips, Phys. Rev. Lett. **95**, 060202 (2005).
[10] S. Curtarolo and G. Ceder, Phys. Rev. Lett. **88**, 255504 (2002).
[11] R. E. Rudd and J. Q. Broughton, Phys. Rev. B **72**, 144104 (2005).
[12] J. Q. Broughton, F. F. Abraham, N. Bernstein, and E. Kaxiras, Phys. Rev. B **60**, 2391 (1999).
[13] H. S. Park, E. G. Karpov, P. A. Klein, and W. K. Liu, J. Comput. Phys. **207**, 588 (2005).
[14] W. A. Curtin and R. E. Miller, Modell. Simul. Mater. Sci. Eng. **11**, R33 (2004).
[15] S. Kohlhoff, P. Gumbsch, and H. F. Fischmeister, Philos. Mag. A **64**, 851 (1991).
[16] S. T. O'Connell and P. A. Thompson, Phys. Rev. E **52**, R5792 (1995).
[17] E. G. Flekkoy, G. Wagner, and J. Feder, Europhys. Lett. **52**, 271 (2000).
[18] X. B. Nie, S. Y. Chen, W. N. E, and M. O. Robbins, J. Fluid Mech. **500**, 55 (2004a).
[19] X. B. Nie, S. Y. Chen, and M. O. Robbins, Phys. Fluids **16**, 3579 (2004).
[20] S. Qu, V. Shastry, W. A. Curtin, and R. E. Miller, Modell. Simul. Mater. Sci. Eng. **13**, 1101 (2005).
[21] D. K. Datta, R. C. Picu, and M. S. Shephard, Int. J. Multiscale Comp. Eng. **2**, 401 (2004).
[22] J. Fish and W. Chen, Comput. Methods Appl. Mech. Eng. **193**, 1693 (2004).
[23] S. P. Xiao and T. Belytschko, Comput. Methods Appl. Mech. Eng. **193**, 1645 (2004).
[24] W. Cai, M. de Koning, V. V. Bulatov, and S. Yip, Phys. Rev. Lett. **85**, 3213 (2000).
[25] W. E and Z. Huang, Phys. Rev. Lett. **87**, 135501 (2001).
[26] W. E and Z. Huang, J. Comput. Phys. **182**, 234 (2002).
[27] J. Z. Yang and X. Li, Phys. Rev. B **73**, 224111 (2006).
[28] L. E. Shilkrot, R. E. Miller, and W. A. Curtin, J. Mech. Phys. Solids **52**, 755 (2004).
[29] B. Shiari, R. E. Miller, and W. A. Curtin, ASME J. Eng. Mater. Technol. **127**, 358 (2005).
[30] S. J. Plimpton, J. Comput. Phys. **117**, 1 (1995).
[31] Http://www.cs.sandia.gov/sjplimp/lammps.html
[32] M. P. Allen and D. J. Tildesley, *Computer Simulation of Liquids* (Clarendon Press, Oxford, 1987).
[33] P. J. Hoogerbruge and M. M. V. A. Koelman, Europhys. Lett. **19**, 155 (1992).
[34] M. O. Robbins and M. H. Müser, in *Handbook of Modern Tribology*, edited by B. Bhushan (CRC Press, Boca Raton, 2000), pp. 717–765.
[35] M. H. Müser and M. O. Robbins, in *Springer Handbook of Nanotechnology* (Springer-Verlag, Berlin, 2004), pp. 717–738.
[36] C. Denniston and M. O. Robbins, Phys. Rev. E **69**, 021505 (2004).
[37] T. J. R. Hughes and T. Belytschko, J. Appl. Mech. **50**, 1033 (1983).
[38] T. J. R. Hughes, *The Finite Element Method: Linear static and dynamic finite element analysis* (Prentice-Hall, Englewood Cliffs, NJ, 1987).
[39] X. B. Nie, M. O. Robbins, and S. Y. Chen, Phys. Rev. Lett. **96**, 134501 (2006).
[40] R. W. Carpick and M. Salmeron, Chem. Rev. (Washington, D.C.) **97**, 1163 (1997).
[41] R. E. Miller, L. E. Shilkrot, and W. A. Curtin, Acta Mater. **52**, 271 (2004).
[42] P. Meakin, *Fractals, Scaling and Growth far from Equilibrium* (Cambridge University Press, Cambridge, England, 1998).
[43] J. Ringlein and M. O. Robbins, Am. J. Phys. **72**, 884 (2004).
[44] M. H. Müser, M. Urbakh, and M. O. Robbins, Adv. Chem. Phys. **126**, 187 (2003).
[45] A. Socoliuc, R. Bennewitz, E. Gnecco, and E. Meyer, Phys. Rev. Lett. **92**, 134301 (2001).